CrossMark

Wear Performance of A356 Matrix Composites Reinforced with Different Types of Reinforcing Particles

Mostafa Akbari, Mohammad Hasan Shojaeefard, Parviz Asadi, and Abolfazl Khalkhali

To improve the wear resistance of Al-Si alloys, different types of reinforcing particles such as SiC, TiC, ZrO_2, and B_4C were used to produce matrix composites by friction stir processing (FSP). First, microstructural properties of different locations of stir zone (SZ) in the FSPed specimens such as advancing side, retreating side, shoulder-affected area, and pin-affected area were investigated. The results demonstrate that Si particles size is not the same in different SZ subdomains. SEM investigation was performed in order to investigate the particles distribution in different areas of the SZ as well as bonding quality between particles and metal matrix. Hardness and wear tests were carried out to determine mechanical and wear properties of the composites. The pin-on-disk wear tests were performed at room temperature, with the normal applied loads of 5, 10, and 20 N and sliding speed of 1 and 2 m/s. All fabricated composites show higher resistance in wear than A356 alloy. Wear test results show, by increasing the normal load and sliding velocity, the wear loss weight of all composites increased gradually.

1. Introduction

Aluminum–silicon alloys are used widely in many industries like automotive and aerospace due to their satisfactory wear resistance and mechanical properties as well as excellent castability (Ref 1-5). They are good choice for internal combustion engine components such as piston, cylinder block, manifold, valve, and connecting rod. However, the wear resistance and mechanical properties of these alloys are limited due to various defects such as porosity, dendritic structure, non-uniformly distributed coarse, and acicular Si particles (Ref 6-10).

For solving this issue, some methods like heat treatment, modifier treatment, and stirring solidification have been developed to refine and enhance microstructure of Al-Si cast alloy (Ref 11). However, none of these methods can uniformly redistribute the Si particles throughout the metal matrix and eliminate defects such as porosity and accordingly cannot enhance the strength and especially ductility of Al-Si alloy (Ref 12). FSP can be used as an effective modification technique for microstructural refinement and a result improving the wear resistance and mechanical properties of these alloys (Ref 3).

FSP has been invented for microstructural modification and improving the mechanical and wear properties of materials

based on friction stir welding (FSW) which has been used to weld different Al (Ref 13), Mg, and Cu alloys (Ref 14, 15), some of which are classified as practically unweldable alloys in use of conventional welding methods (Ref 16-18).

Several methods have been employed to fabricate of surface composites such as ion implantation methods (Ref 19), plasma spraying methods (Ref 20), micro-arc oxidation methods (Ref 21), and laser cladding methods (Ref 22). However, the laser cladding technology involves liquid-phase processing at high temperatures, which may result in an interfacial reaction between the metal matrix and reinforcing particles (Ref 23). Additionally, in order to achieve an appropriate microstructure, the precise control of processing parameters is needed. On the other side, spraying or micro-arc oxidation techniques for the surface composite fabrication reveal an obvious stratification between the surface layer and the base metal, leading to a weakness in the interfacial bonding strength (Ref 23). The surface composite layer produced by the ion implantation method is only in the scale of a few hundred nanometers. FSP has demonstrated its potential in fabrication of different and widely used surface composites with little or no interfacial reaction with the reinforcements (Ref 24). This process also produces a thermo-mechanically refined microstructure that have superior properties including a dense solid without porosity, uniform dispersion of reinforcing particles in the metal matrix, and strong bonding between reinforcing particles and matrix compared to conventional methods. These advantages have been especially used for surface composites fabrication in order to homogenize the microstructure of reinforcing particles deposited on the surface of a base alloy. Although FSP has several advantages for composite fabrication, some issues have limited this method. First of all, FSP is a surface composite fabrication method and it is hard to use this method for fabrication of bulk composites. Moreover, for FSP some preprocessing operations including groove machining, particles embedding, and surface closing are needed that make this method time-consuming. FSP has the potential to be used where the enhanced properties of such microstruc-

Mostafa Akbari and **Abolfazl Khalkhali**, School of Automotive Engineering, Iran University of Science and Technology, Tehran, Iran; **Mohammad Hasan Shojaeefard**, School of Mechanical Engineering, Iran University of Science and Technology, Tehran, Iran; and **Parviz Asadi**, Department of Mechanical Engineering, Faculty of Engineering, Imam Khomeini International University, Qazvin, Iran; Contact e-mail: mr.mostafaakbari@yahoo.com.

tures are only required in localized regions, for example, on the cutting edges of blades or the contact surfaces of ring bearing races.

Until now, FSP has been used to fabricated the composites with different types of reinforcing particles including SiC (Ref 10, 23), TiC (Ref 24), Al_2O_3 (Ref 25), CNT (Ref 26-28), TiO_2 (Ref 29) and B_4C (Ref 30). Shojaeefard et al. (Ref 25) fabricated boron carbide/aluminum composites on an aluminum–silicon cast alloy using FSP. They showed that the hardness and wear resistance of the composite significantly improved compared with base alloy. Asadi et al. (Ref 24) added SiC nanoparticles to as-cast AZ91 magnesium alloy and produced AZ91/SiC surface nanocomposite layer. Although a numerous works have been done on this subject, investigation of the effect of reinforcing particles type on the mechanical properties and wear resistance of A356 matrix composites is of great interest to be considered. Most of previous works has only considered the effect of one or two reinforcement on properties of fabricated composites. In this investigation, several composites reinforced by different types of reinforcing particles were produced in order to select the best reinforcing particles with the aim of improving the hardness and wear resistance of the A356 aluminum alloy.

In this study, the material flow during FSP is numerically modeled using a thermo-mechanically coupled rigid viscoplastic 3D FEM (Ref 18, 26-31). Recently, some researchers have attempted to develop numerical model for material flow during FSW/FSP. Marzban et al. (Ref 27) studied the effect of pin profile on material flow and strain distributions during friction stir welding of AA5083. They concluded that only the material in the advancing side entered inside the SZ when tool with cylindrical pin profile was used, while for the square pin profile, both advancing and retreating sides entered the SZ. Shojaeefard et al. (Ref 31) used 3D FEM analysis to investigate the effect of tool rotational and traverse speeds on peak temperature and welding force.

In this study, in order to improve the wear resistance of Al-Si alloy, different types of reinforcing particles such as SiC, TiC, ZrO_2, and B_4C were used to produce matrix composites by friction stir processing method. SEM investigation was performed in order to investigate the particles distribution in different regions of the FSP parts as well as bonding quality between particles and metal matrix. Hardness and wear tests were carried out to determine mechanical and wear properties of the composites. The pin-on-disk wear tests were performed at room temperature, with the normal applied loads of 5, 10, and 20 N and sliding speeds of 1 and 2 m/s.

2. Experimental Method

Fabrication of composites was performed on A356 alloy, containing 7% Si, 0.31% Fe, 0.10% Mn, 0.35% Mg, 0.1% Zn, and balance Al. In order to study the effect of reinforcing particles type on wear resistance of the composites, various particulate reinforcements including ZrO_2, SiC, B_4C, and TiC were used (Ref 25, 32, 33). The specifications of reinforcements are summarized in Table 1. The average volume fraction of particles in the composites was 12%.

For composite fabrication, first, a groove was machined in the surface of an aluminum plate. Then, different reinforcing particles were embedded into the groove. After that, a pin-less tool was utilized to seal the groove surface in order to prevent the particles escapement during the FSP. Finally, the plate was processed by FSP for four passes along the groove.

In this study, FSP tool with threaded pin profiles was used to fabricate the composites. Based on author pervious works, threaded pin profile can uniformly distribute particles at SZ in comparison with other pin profiles. FSP pin and shoulder diameters are 6 and 18 mm, respectively. In all experiments, the composites were produced at constant tool tilt angle and penetration depth of 3° and 3.5 mm, respectively.

The microstructure of FSPed specimens was investigated by a metallurgical microscope and SEM.

The specimens were mechanically polished and etched with Keller's reagent according to the standard metallographic procedures. The micro-hardness tests were carried out at the stir zone (SZ) with normal load and dwell time of 200 g and 15 s, respectively. For each composite the hardness of 5 points was measured and their average value was reported.

A four-channeled thermometer with the accuracy of ±0.1 °C was employed to record temperature history for special points during the FSP. A K-type thermocouple was embedded at 15-mm distance from the center line in order to measure temperature.

To obtain the axial force history over the process usually in order to validate FEM model, a specially designed load measuring system was used (Fig. 1). This dynamometer benefits from two bending load cells for measuring axial force with an accuracy of 1.2 kg at sampling rate of 10 samples per second. The signal was interfaced with a PC through various signal conditioning devices, and the results were saved as an excel spread sheet using a MATLAB program.

To study the wear resistance of the composites, wear tests were performed on an IUST@WS116 pin-on-disk tribometer produced by IUST research group (Ref 34). The pin specimens with diameter of 6 mm were cut from the surface of the composites. The wear tests were conducted against a counterpart disk made of 2080 steel alloy with hardness of 60 HRC and surface roughness of about 0.5 μm. The wear tests were carried out under different normal loads of 5, 10, and 20 N and different sliding speeds of 1 and 2 m/s. Moreover, all wear tests were done at room temperature.

## 3. Numerical Model of Friction Stir Processing

In order to simulate the material flow during FSP, Deform-$3D_{TM}$ software was employed due to its good capability in modeling severe plastic deformation (SPD) processes (Ref 1, 35). The workpiece was considered as rigid viscoplastic, while the tool as rigid material.

Friction between FSP tool and workpiece was modeled via the constant shear friction model of $f = mk$ (Ref 35, 36). In this equation f represents the frictional stress, k is the shear yield stress, and m is the friction factor. Comparison between temperature history derived from the simulation and experimental results shows a good agreement between the experimental and predicted data (Fig. 2).

A non-uniform meshing with automatic remeshing for the tool and workpiece was used in about 20,000 and 90,000 tetrahedral elements, respectively. The finer elements in the mean size of 0.5 mm were placed under the tool pin. The workpiece and the tool models are shown in Fig. 3. More

Table 1 Specifications of different reinforcements

	Density, g cm^{-3}	Thermal expansion, 10–6/°C	Thermal expansion difference	Hardness, kg mm^{-2}	References
ZrO$_2$	6	10.3	11.9	1300	Ref 29
B$_4$C	2.52	5	17.2	2800	Ref 22
TiC	6	7.4	14.8	3200	Ref 30
SiC	3.16	4	18.2	2800	Ref 30
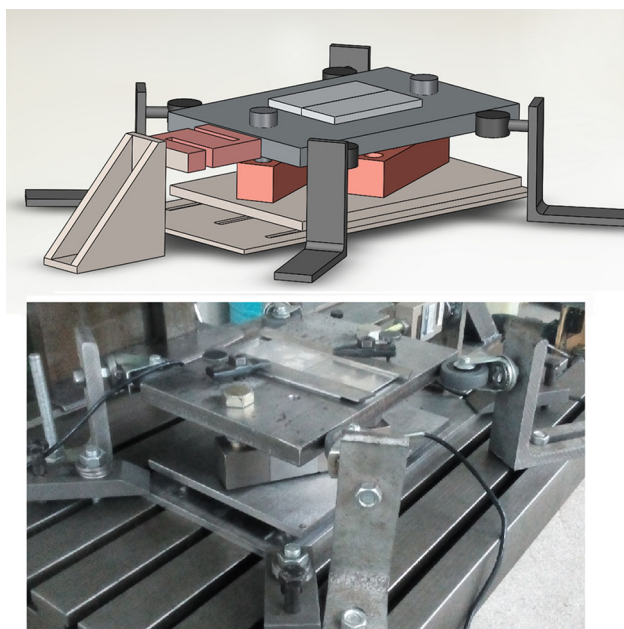
Fig. 1 FSW fixture with mounted force measuring system
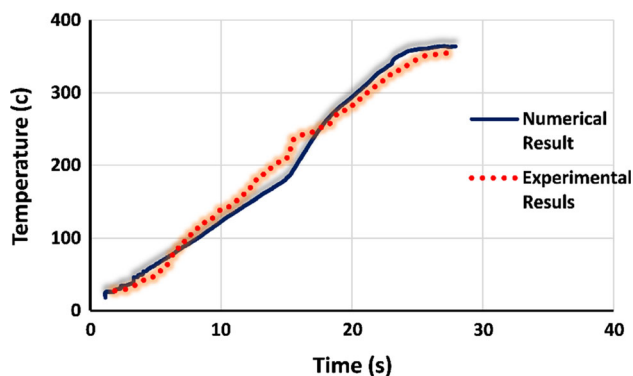
Fig. 2 Temperature history obtained from the FEM and experimental results

details on FEM model can be found in our pervious works (Ref 18, 24, 26-28, 30, 31, 37).

4. Results and Discussion

In the present study, the effects of different reinforcing particles on the microstructure, hardness, and wear resistance of surface composite layers produced by FSP are examined. Besides the material properties, the material flow occurred during the process is investigated as well. The results of different examinations are reported and discussed in the following sections.

## 4.1 Microstructural Results and Particles Distribution

The microstructures of A356 base alloy are shown in Fig. 4(d), where the existence of coarse needle-like Si particles in the base metal can be observed obviously. Also, distribution of the Si particles overall the Al matrix is not uniform. The mean size of Si particles in the base alloy is about 10.04 μm, with the mean aspect ratio of 4.67. These large hard components with very high aspect ratio and sharp ends lead to the brittle behavior of the alloy. FSP, as a microstructural modifying process, has demonstrated its capability in refining different hard components such as dendrites (Ref 25) and intermetallics (Ref 34) in the microstructures of alloys. Figure 4(b) shows the microstructures for different zones of the FSPed specimen without the reinforcing particles. Two distinct zones have been identified: stirred zone (nugget) and thermo-mechanically affected zone (TMAZ). In this study, the heat-affected zone (HAZ) microstructure was found very similar to that of the BM. The coarse needle-like silicon particles are broken up and uniformly distributed in the SZ as a result of stirring action of the rotating tool and derived severe plastic deformation (Fig. 4c). Elimination of the large and sharp-ended Si components will weaken the frangibility of A356 Alloy. The mean size and aspect ratio of Si components are dropped down to about 1 μm and 1.5, respectively.

Figure 4(c) illustrates the distinct microstructure at the boundary throughout the transition zone between the SZ and the BM where Si particles are bigger than that of in the SZ and smaller than Si particles at BM. This transition zone can be related to the thermo-mechanically affected zone (Fig. 4e). The common feature of this region is elongated or rotated grains, and recrystallization does not happen in this area because of inadequate heat and plastic deformation. Moreover, at this region, Si particles were dispersed in an upward flowing pattern around the SZ. From Fig. 4(e), it can be understood that materials at TMAZ experienced lower temperature and strain compare with the SZ resulted in generation bigger Si particles. The peak strain at TMAZ is about 14, significantly lower than that at SZ which is 50 as shown in Fig. 4(a).

Microstructure and material flow of different sides of SZ, namely advancing and retreating sides, are shown in Fig. 5(c), (d). In order to investigate material flow at both sides, some points were marked at AS an RS as shown in Fig. 5(a). Points P1 to P6 and P7 to P12 are placed in steps of 0.4 mm from the tool pin at the retreating and advancing sides, respectively. From this figure, it can be concluded that points placed at the advancing side, rotated with the tool pin from the front to the back of the pin, and finally placed at the advancing side again. As a result, materials with maximum distances of 1.6 mm (points P7–P10) from the pin enter to the SZ. This material flow characteristic at AS is the main reason for broadening the SZ at
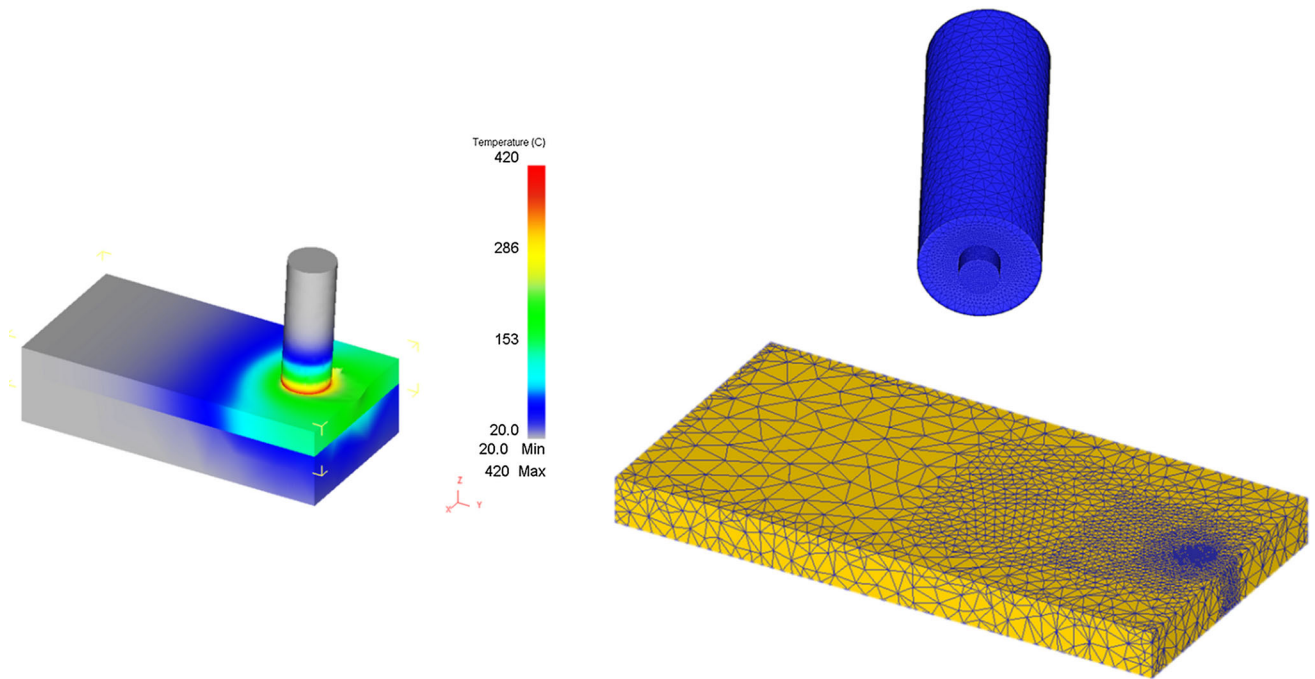
Fig. 3 Schematic illustration of tool and workpiece in the finite element model
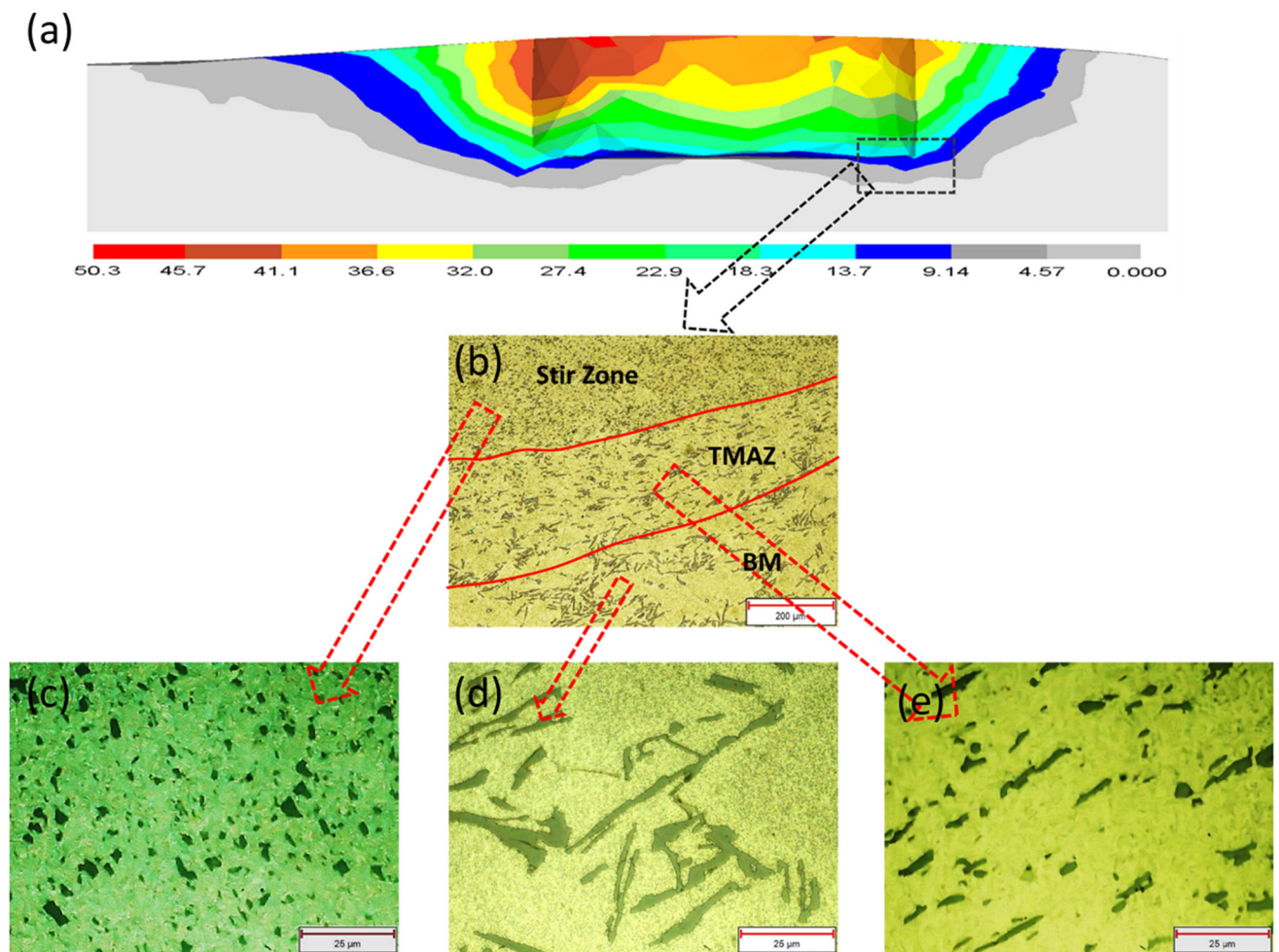
Fig. 4 Microstructures observed for different zones in the FSPed specimen

the AS, as shown in Fig. 5(c). Displacement of points P11–P12 is much less than the displacement of points P7–P10, and it can be concluded that these points are belonged to the TMAZ. At RS, the materials (i.e., points P1–P6) do not revolve with tool pin and only move in backward direction. Similar observation was also reported by Marzban et al. (2014) that materials at retreating side do not revolve around the pin and enter into the stir zone. Consequently, it can be concluded that the advancing side experiences more shearing of material than the retreating side.

Figure 5(b) illustrates the effective strain contours on the cross section of the FSP samples. It can be seen that materials at the AS experience higher amount of effective strain than at the RS. As discussed before, the amount of material shearing at the AS is higher than that at the RS. Therefore, higher effective strain is expected at the AS. The effective strain in the cross section decreases by moving from the top surface toward the bottom surface. Therefore, the material deformation near the top surface is higher than the near bottom area which results in a conic shape for the SZ.

Microstructures of advancing and retreating sides are shown in Fig. 5(d), (f). As shown from this figure, Si particles at AS are smaller than that in RS. This may be due to higher amount of strains at AS (as stated before) that results in more disruption of Si particles. Moreover, the TMAZ area at AS is wider than that at RS. As shown in Fig. 5(e), the area where materials experience effective strain is broaden at the AS leading to the increased SZ and TMAZ areas at this side.

4.2 SEM Investigation of the Composites

Obtaining homogenous distribution of reinforcing particles in the composites is challengeable. Agglomeration of particles is a major problem in composite production as it worsens the mechanical properties of composites (Ref 38). To investigate the particles distribution in different regions of the SZ, the SEM images of the composite reinforced by B_4C are shown in Fig. 6(b), (c), and (d). Four distinct zones have been identified: AS, RS, shoulder-driven, and pin-driven material flow zones (Fig. 6b). As shown in Fig. 6(c) and (d), the particles distribution at AS and RS is the same and no difference can be observed. This may be due to the fact that in this study the tool rotational direction was changed between each pass leading to change in the flow pattern of the material which improves the particles distribution. By changing the tool rotational direction, AS and RS locations changed together in the tandem passes (Ref 24). As a result, reversing the rotational direction reduces the differences between the AS and RS structures and particle distribution patterns.

Moreover, rich band at the root of pin-driven zone shows that the percentages of reinforcing particles at shoulder-driven and pin-driven zones are different (Fig. 6b). Such a variation from shoulder-driven zone to pin-driven zone can be related to
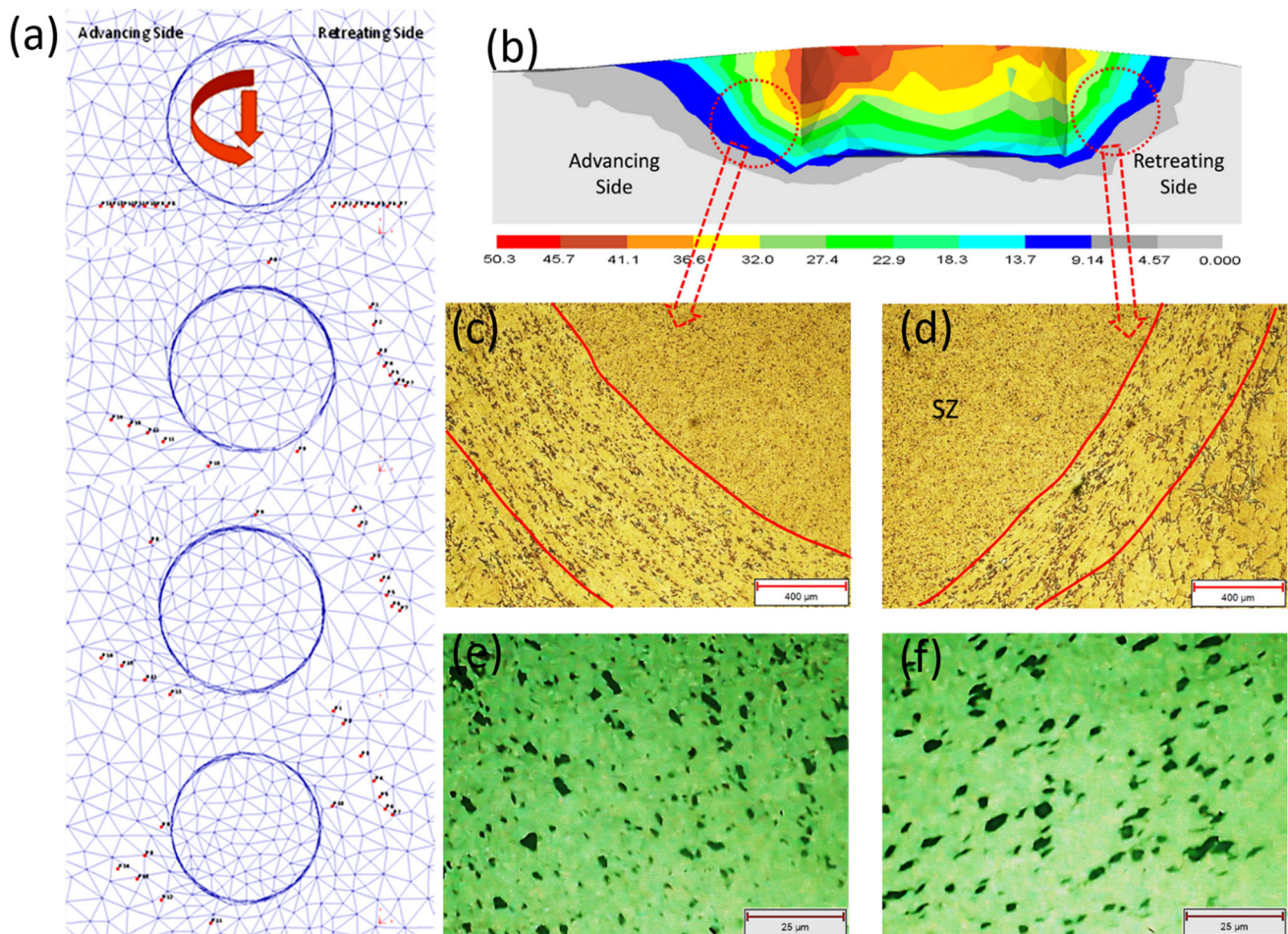
Fig. 5 Comparison between the microstructural and material flow at different side of SZ
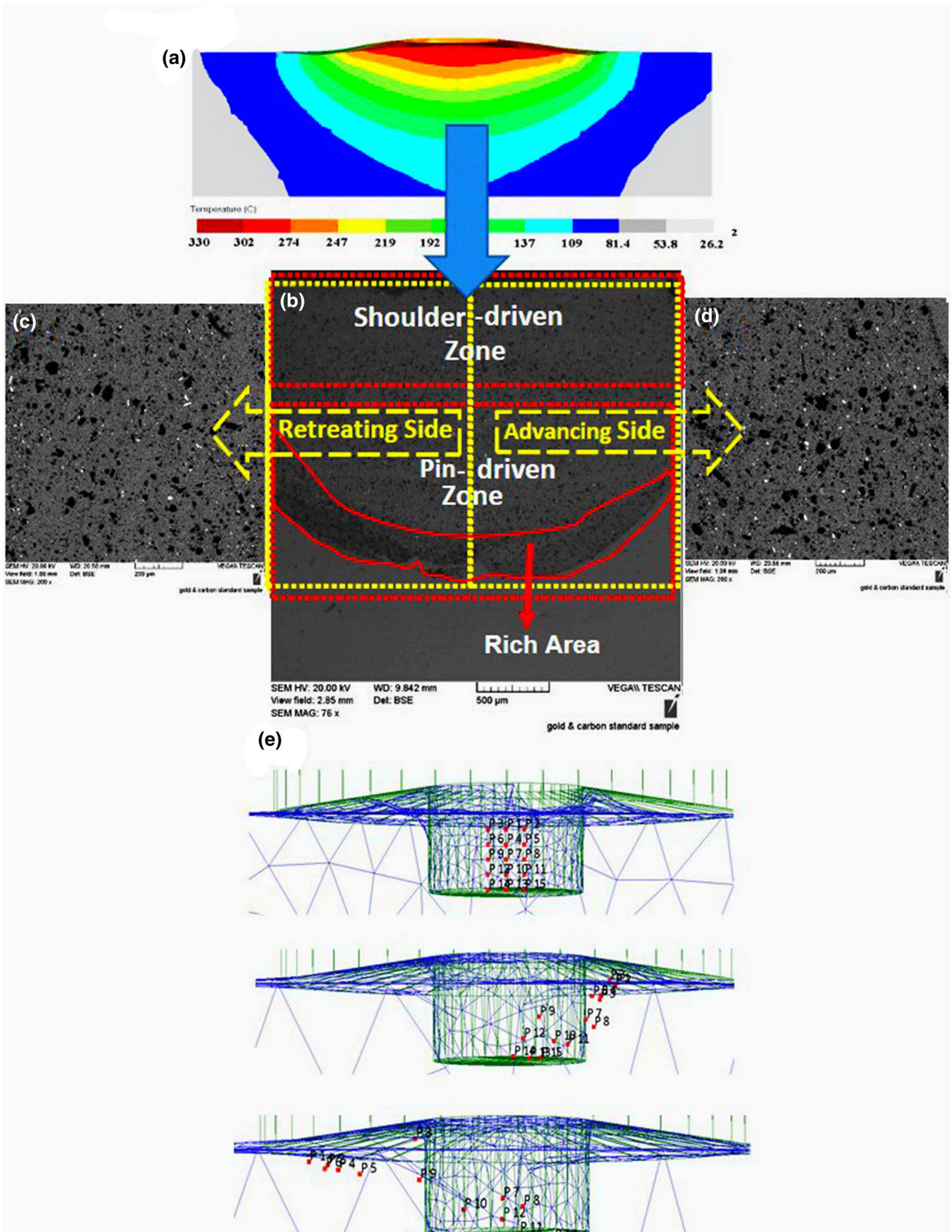
Fig. 6 Cross section of the FSPed sample in the (a) simulation model and (b) real sample. Particle distribution in the (c) RS and (d) AS zone. (e) Material flow pattern in the SZ

different material flow patterns as well as different temperature histories between shoulder-driven and pin-driven zones. In order to further investigation particles dispersion pattern in the metal matrix, material flow generated by circular pin profile during FSP was considered using a simulation model by locating some points inside the SZ to trace the material movements (Fig. 6e).

Figure 6(e) illustrates the material flow during FSP at the points near to the center of workpiece. The points are located along and around the center line very like to the position of the reinforcing particles inserted in the path of tool traveling line, to investigate the particle movement over the FSP and find the final powder distribution pattern after FSP. As it could be observed, the bottom points revolve from the front to the back of the pin, but their position at the center of SZ remains almost constant. However, the points near to the top surface rotate with the pin around the tool axis first to the retreating side and finally toward the advancing side. It can be concluded that by decreasing the distance from the top surface, the stretching of the material toward AS increases. The material modeling revealed that two material flow patterns (namely shoulder-driven flow and pin-driven flow) exist over the FSP. The more material flow at the top surface occurs dominantly due to the influence of the tool shoulder. The maximum material flow was observed in this region, and by increasing the distance from the top surface, a drastic reduction in the material flow was found. As stated before, the percentage of particles at pin-driven zone, especially at pin root, is higher than shoulder-driven zone. This is related to weak material flow at SZ root resulting in a non-uniform distribution and agglomeration of particles in this area.

For further investigation of the particles distribution at different FSP zones, quantitative metallography was done using Image Analyzer software and the results are summarized in Table 2. In the table, the presence of particles in the composite layer is reported in percent of particles per μm^2. As can be concluded, the difference in reinforcing particles percentages at the advancing and retreating sides is only about 1 percent showing a uniform particle distribution in these areas. Moreover, as shown from this table the percentage of reinforcing particles at SZ root is higher than that for other zones due to weak material flow in this zone. However, this difference is only about 3% that can represent a good distribution at whole FSP zones.

Moreover, in order to show the effectiveness of FSP method in distribution of reinforcing particles in metal matrix, it is interesting to compare the particles distribution in composites fabricated by FSP with those of the composites fabricated through other methods.

Mazaheri et al. (Ref 39) fabricated A356 matrix composites reinforced with different volume fractions of B_4C particles via squeeze casting method. They reported that due to the casting process, the reinforcing particles were dispersed between the dendrite branches and were frequently clustered together leaving the dendrite branches as particle-free regions in the material and as a result distribution of the B_4C particles was obviously not uniform. However, in this study as the dendritic microstructure was annihilated due to sever plastic deformation, the reinforcing particles were distributed at whole metal matrix. Moreover, in another research that was done by Sajjadi et al. (Ref 40), the composites ($A356/Al_2O_3$) with different weight percentages of reinforcing particles were produced by two melting methods, namely stir casting and compo-casting. They reported that reinforcing particles have a tendency to segregate and cluster at inter-dendritic regions which are surrounded by eutectic silicon, and particles agglomeration was observed in Al matrix. Carvalho et al. (Ref 41) produced Al-Si/CNT composites by hot pressing powder metallurgy technique. They reported that reinforcing agglomeration existed in the fabricated composites. Izadi et al. (Ref 42) applied FSP to modify the microstructure of Al/SiC composites fabricated by powder metallurgy. They reported that FSP could improve the SiC particles dispersion in the composite. Generally, it can be mentioned that the FSP can uniformly disperse reinforcing particles in the metal matrix due to the severe plastic deformation accompanied by high temperatures over the process (Ref 25, 43).

To study the particles distribution and bonding in the aluminum metal matrix, the SEM images of the composites fabricated by different particles are illustrated in Fig. 7.

One of the most important factors that affect composites properties is strength of bonding between the metal matrix and the reinforcing particles. Strengthening by the reinforcing particles in the composites is severely relying on the strength of the bond between the reinforcement and the metal matrix. As shown in Fig. 7, the reinforcing particles are distributed uniformly in the metal matrix. Moreover, no micro-voids can be clearly observed at the interface between B_4C-, TiC-, and ZrO_2-reinforcing particles and the aluminum metal matrix. As a result, a proper reinforcing/matrix bonds are obtained for these composites.

On the other hand, it is demonstrated that the micro-voids are existed around the SiC particle which can be as a result of the poor wettability of the SiC particles in the aluminum matrix (Fig. 7d).

4.3 Hardness in the Cross Section of Surface Composites

The average hardness of the composites produced by different types of particles is shown in Fig. 8. As can be understood from this figure, hardness of all composites is increased significantly compared with that of the base alloy.

Table 2 Particles percentage at different FSP zones

FSP zone	Phase	Particles percent, % per μm^2
Advancing side	Reinforcing particles phase	9.87
	Retained phase	90.12861
Retreating side	Reinforcing particles phase	8.89
	Retained phase	91.10943
Pin root	Reinforcing particles phase	13.36
	Retained phase	86.64176
Shoulder-driven area	Reinforcing particles phase	9.45
	Retained phase	90.55
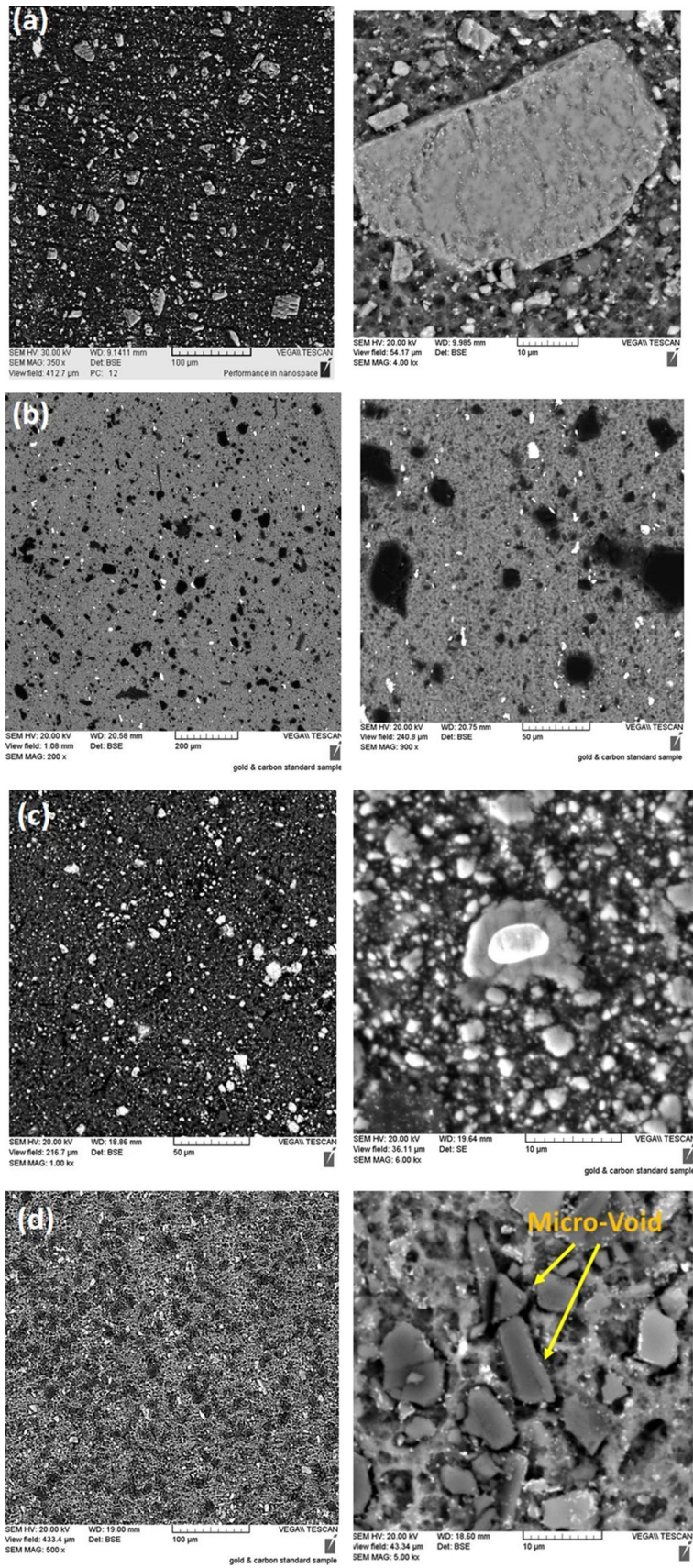
Fig. 7 SEM micrographs from the A356 Al based composites fabricated with different reinforcements of (a) TiC, (b) ZrO$_2$, (c) B$_4$C, and (d) SiC

However, the effect of different reinforcing particles in raising the composite hardness is different. Using TiC as reinforcing particles resulted in achieving the highest hardness value in comparison with using other reinforcing particles. TiC-reinforced composite, with the hardness of 150 HV, exhibits rather high hardness in comparison with other composites fabricated in this study. Based on previous studies (Ref 32), difference in hardness value of different composites fabricated in a same matrix but by different reinforcements may be related to several factors such as reinforcement hardness, thermal expansion difference between matrix and reinforcing particles, as well as matrix/reinforcement bonding quality.

Thermal expansion coefficient difference between the matrix and the reinforcing particles is one since generating dislocations during the heating/cooling over the process affects the strength and hardness of the composites (Ref 44). Considering this factor (as shown in Table 2), it was expected the hardness value
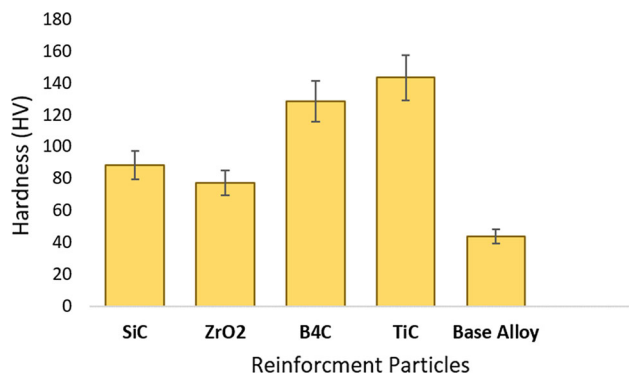

Fig. 8 Average micro-hardness value for the composites produced with different particle reinforcements

of the composites reinforced by SiC would be maximum. However, its hardness is just higher than the ZrO_2-reinforced composite, and other factors may be affected more severely the hardness value of composites.

The other factor is bonding strength in the matrix/reinforcement interface as discussed before. The poor bonding between SiC particles and Al matrix is a major factor lowering the composite hardness (Fig. 7d).

Considering the TiC- and B_4C-reinforced composites, although the thermal expansion coefficient difference between B_4C and the metal matrix is higher than that for TiC, and both the TiC and B_4C have good bonding with the metal matrix, the hardness of TiC-reinforced composite is higher. This may be resulted from the higher hardness of TiC reinforcement itself (Table 1).

The Al/ZrO_2 composite has the lowest hardness as compared with the other composites, while ZrO_2 has a well bonding with the metal matrix (Fig. 7b). Indeed, ZrO_2 involves the lowest amount for both the hardness and the thermal expansion difference among the reinforcing particles used in this study. This leads to having the lowest composite hardness.

4.4 Wear and Friction Performance of Fabricated Composites

Since the hardness values of different composites produced by addition of several reinforcements are different, it is expected that the wear resistance of composites will be different as well. In the following subsections, effects of reinforcing particles type, normal load, and sliding speed on wear properties of fabricated composites are considered.

4.4.1 Influence of Reinforcing Particles Type on Wear and Friction Performance. The wear and friction properties of composites reinforced via different types of particles are shown in Fig. 9. All composites show better wear properties in
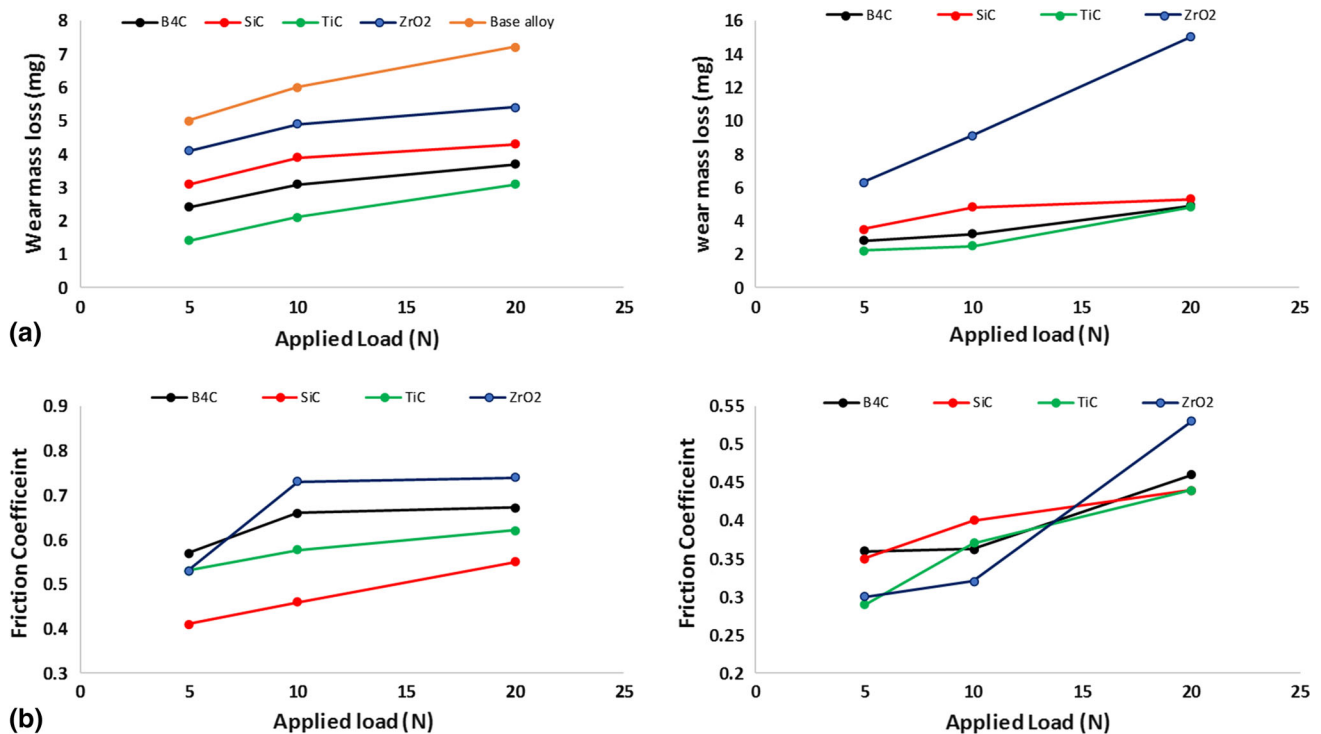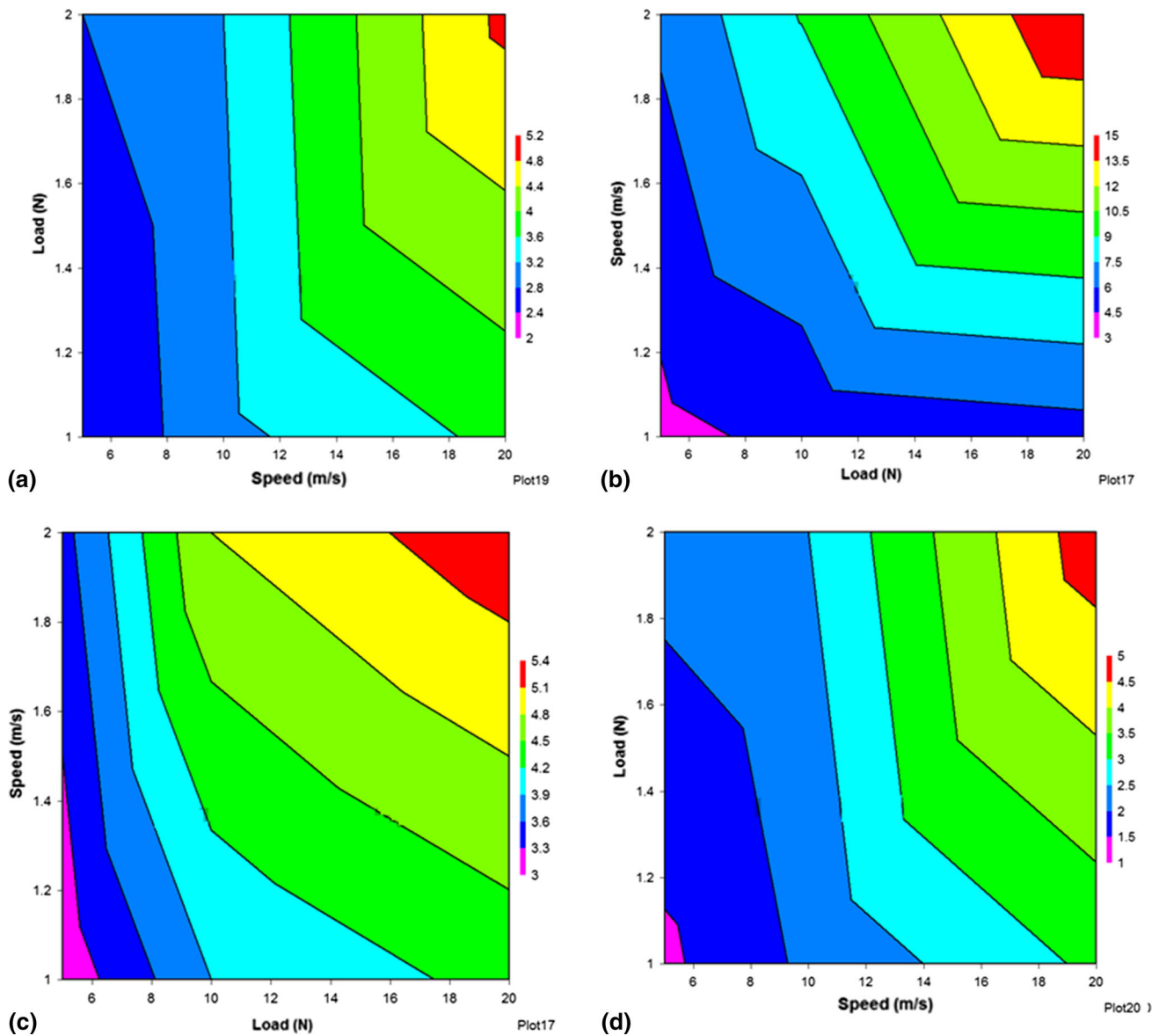

Fig. 9 Wear and friction properties of composites at sliding speed of (a) 1 m/s and (b) 2 m/s

Fig. 10 Contour plot showing the wear mass loss of composites reinforced with (a) B$_4$C, (b) ZrO$_2$, (c) SiC, and (d) TiC

comparison with A356 base alloy. Generally, particles act as load bearing components because of their high hardness value and lead to significantly reduction in the contact area between the composites and counterpart disk leading to an increase in wear resistance of the composites (Ref 45, 46). Moreover, the wear loss weight of different composites shows a similar trend with the hardness of the composites. The composite reinforced by TiC and ZrO$_2$ particles exhibited the highest and the lowest wear resistances among the fabricated composites. According to the Archard equation, an increase in the hardness value of the composites leads to an improvement in the wear resistance of the composites (Ref 46, 47).

Figure 9 illustrates the variation of the friction coefficient for composite reinforced with different reinforcing particles at different applied loads and sliding velocities. At lower sliding speed, the composite reinforced with SiC particles has the lowest average friction coefficient. This may be due to the poor bonding between the particles and the metal matrix that leads to easily removal of the reinforcement particles during test (Ref 32).

4.4.2 Influence of Normal Load and Sliding Speed on Wear and Friction Performance. To elucidate the combined effect of normal loads and sliding velocity on wear resistance of different composites, maps showing variation of wear loss weight and friction coefficient with respect to both these parameters are illustrated in Fig. 10 and 11. These maps obviously demarcate different regions with varying friction coefficient and wear mass loss. As shown in the figures with the normal load increasing, the wear mass loss of all composites increased gradually. At the higher applied load, the composites are forced against the disk leading to temperature increase at the interface and consequently destroying the transfer film at a faster rate (Ref 48). So new transfer films are formed at faster rate enhancing the wear of the lining. These findings are in agreement with Archard equation of wear that states the wear is low at lower value of applied loads and increases with load at a constant ratio.

Moreover, in most cases the increase in the applied load leads to rise in friction. The friction coefficient is observed as a higher amount at higher applied loads, because at lower applied
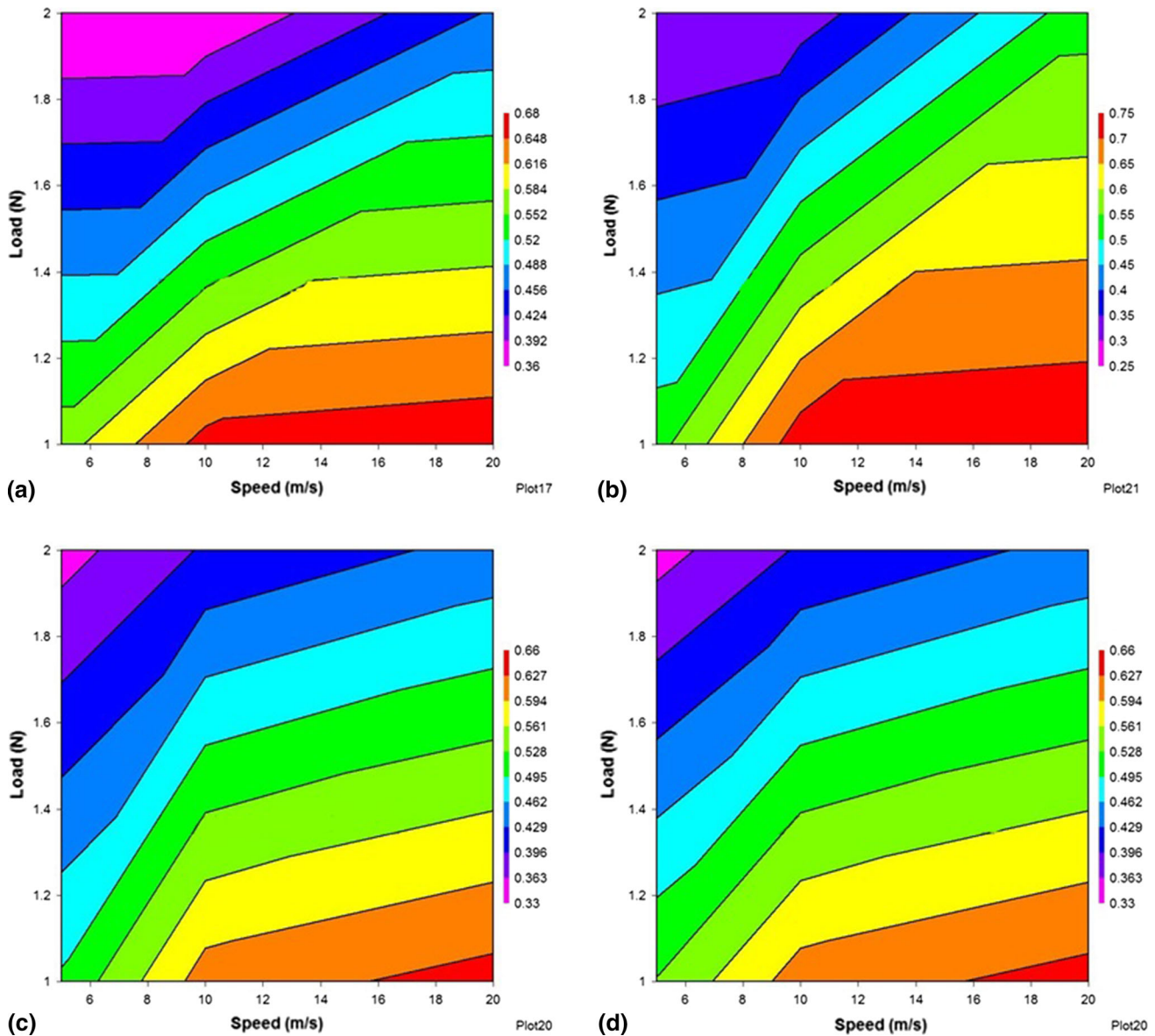
Fig. 11 Contour plot showing the friction coefficient of composites reinforced with (a) B$_4$C, (b) ZrO$_2$, (c) SiC, and (d) TiC

loads, the transfer film is more stable and temperature rise is also low, whereas at higher loads the transfer film is destroyed at faster rate.

Moreover, Al-Si alloy easily is oxidized when is exposed to the air in the initial duration of wear test. An increase in the applied load results in an increased wear and a loss of the metal as stated before. The initial rubbing duration breaks the surface layers, which cleans and smoothens the surfaces and increases the strength of the connections and contact between the surfaces. The friction force due to the tillage effect between the surfaces increases the temperature at the interface. This effect results in adhesion and increases the deformation at the surface layers, leading to further increase in friction.

Moreover, it is interesting to compare the wear properties of the composites fabricated by FSP with those of the composites fabricated through other methods. Alpas and Zhang (Ref 49) investigated the effect of SiC particulate reinforcement on the dry sliding wear of A356 composites produced by the Dural process. They measured wear rates of the composites over a various loads range. They concluded that an increase in amount of applied load leads to an increase in wear rate of the composite, and that is in line with results of this study. However, they reported that at a low applied load (< 10 N) the composite exhibited a lower wear rate than the unreinforced alloy and at 'medium' load levels between 10 and 95 N, and both the unreinforced alloy and the alloys incorporating SiC particles exhibited similar wear behavior. Uthayakumar et al. (Ref 50) investigated wear properties of A356 unreinforced alloy as well as composites with different vol.% of boron carbide particles. They evaluated that the wear properties of the hybrid composites were over a load ranges of 20-100 N, at the sliding velocities from 1 to 5 m/s. They reported that aluminum pin is showing the continuously increasing trend of wear with increasing normal load due to direct metal to metal contact.

It can be understood from Fig. 10 that maximum mass loss occurs at the highest velocity and it decreases with the decrease in the sliding velocity for all composites. It can be due to this fact that by increasing the sliding velocity of counterpart disk,
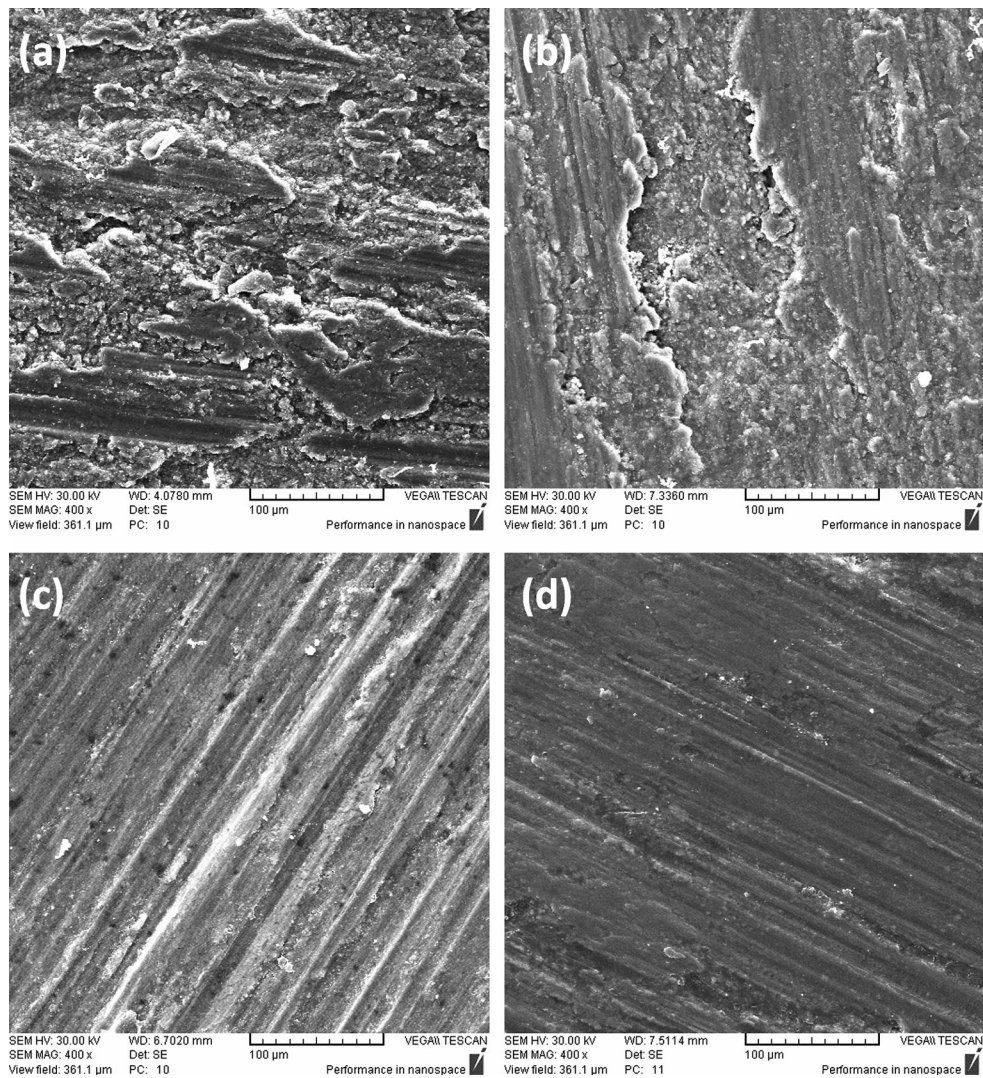
Fig. 12 SEM micrograph of the worn surface in the composite reinforced with (a) ZrO$_2$, (b) SiC, (c) B$_4$C, and (d) TiC

temperature of the specimen increases resulting in adhesion and increase in the deformation at the interface. Natarajan et al. (Ref 51) investigated wear behavior of A356/25SiCp aluminum matrix composites produced by stir casting. They observed similar trend when they studied the effect of sliding speed on wear properties of material.

Additionally, as shown in Fig. 12, the friction coefficient of all composites decreased by increasing sliding speed, and this is just contrary to the wear. This may be due to the fact that at higher velocity, the formation or destruction of the transfer film is fast which results in the reduced friction coefficient.

Figure 12 illustrates the SEM micrographs of the worn surface of the composites reinforced by different particles type. For the Al/SiC and Al/ZrO2, many parallel grooves and delamination were found which illustrates that both delamination and abrasive mechanisms are the dominant wear mechanisms. Additionally, the pits are predominantly existed in the wear track of the composite reinforced by SiC because of reinforcing particles removal. The plowed grooves in the worn surface of the Al/TiC and Al/B$_4$C composites reveal that the abrasive wear component is taken place. Presence of the hard reinforcing particles and high quality of the particles/matrix bonding in the composites reinforced with TiC and B$_4$C

particles prevented the adhesive wearing and drastic material removal. Moreover, the wear specimen surface of the composite fabricated by TiC is smoother than that for the Al-B$_4$C composite verifying the higher wear resistance of the Al/TiC composite.

5. Conclusion

In this study in order to improve the wear resistance of Al-Si alloys, different types of reinforcing particles such as SiC, TiC, ZrO$_2$, and B$_4$C were used to produce matrix composites by friction stir processing method. First, microstructural properties of different areas inside the stir zone (SZ) of FSPed specimens such as advancing side (AS), retreating side (RS), shoulder-affected area, and pin-affected area were investigated. SEM investigation was performed to consider the particles distribution in different areas of the FSPed specimens as well as bonding quality between particles and composite matrix. The pin-on-disk wear tests were performed with several normal loads and sliding speeds. In summary, the following conclusions were reached:

- Based on Si particles size, three distinct zones can be identified: stirred zone (nugget), thermo-mechanically affected zone (TMAZ), and base metal (BM).
- Four different SZ subdomains were identified, namely shoulder-driven zone, pin-driven zone, advancing side, and retreating side.
- Difference in hardness value of composites fabricated by different reinforcements is attributed to several factors including hardness, particles size, and thermal expansion of reinforcements and bonding quality in reinforcement/matrix interface.
- As the normal load increases, the wear mass loss of all composites increases.
- The friction coefficient is observed as a higher amount at higher applied loads.
- The maximum mass loss occurs at the highest velocity, and it decreases with the decrease in the sliding velocity for all composites.
- The percentage of reinforcing particles at SZ root is higher than that for other zones due to weak material flow in this zone.
- Maximum hardness was obtained in the Al/TiC composite (about 150 HV) because of the excellent bonding between TiC reinforcing particles and metal matrix as well as higher hardness value of reinforcement itself compared with the other reinforcements.

References

1. S. Tutunchilar et al., Simulation of Material Flow in Friction Stir Processing of a Cast Al-Si Alloy, *Mater. Des.*, 2012, **40**, p 415–426
2. V.C. Srivastava, R.K. Mandal, and S.N. Ojha, Microstructure and Mechanical Properties of Al-Si Alloys Produced by Spray Forming Process, *Mater. Sci. Eng. A*, 2001, **304–306**, p 555–558
3. S.A. Alidokht et al., Evaluation of Microstructure and Wear Behavior of Friction Stir Processed Cast Aluminum Alloy, *Mater. Charact.*, 2012, **63**, p 90–97
4. M.O. Shabani et al., Wear Properties of Rheo-Squeeze Cast Aluminum Matrix Reinforced with Nano Particulates, *Prot. Met. Phys. Chem. Surf.*, 2016, **52**(3), p 486–491
5. M.O. Shabani et al., Superior Tribological Properties of Particulate Aluminum Matrix Nano Composites, *Prot. Met. Phys. Chem. Surf.*, 2016, **52**(2), p 244–248
6. V. Vijeesh and K.N. Prabhu, Review of Microstructure Evolution in Hypereutectic Al-Si Alloys and Its Effect on Wear Properties, *Trans. Indian Inst. Met.*, 2014, **67**(1), p 1–18
7. J. Clarke and A.D. Sarkar, Wear Characteristics of As-Cast Binary Aluminium-Silicon Alloys, *Wear*, 1979, **54**(1), p 7–16
8. B.K. Prasad et al., Sliding Wear Behavior of Some Al-Si Alloys: Role of Shape and Size of Si Particles and Test Conditions, *Metall. Mater. Trans. A*, 1998, **29**(11), p 2747–2752
9. M. Shamsipour et al., Optimization of the EMS Process Parameters in Compocasting of High-Wear-Resistant Al-Nano-TiC Composites, *Appl. Phys. A*, 2016, **122**(4), p 457
10. M. Akbari et al. Effect of Tool Parameters on Mechanical Properties, Temperature, and Force Generation During FSW, in *Proceedings of the Institution of Mechanical Engineers, Part L: Journal of Materials: Design and Applications* (2016), p. 1464420716681591
11. S. Tutunchilar et al., Eutectic Al-Si Piston Alloy Surface Transformed to Modified Hypereutectic Alloy Via FSP, *Mater. Sci. Eng. A*, 2012, **534**, p 557–567
12. M. Akbari et al. Wear and Mechanical Properties of Surface Hybrid Metal Matrix Composites on Al-Si Aluminum Alloys Fabricated by Friction Stir Processing, in *Proceedings of the Institution of Mechanical Engineers, Part L: Journal of Materials: Design and Applications* (2017), p. 1464420717702413
13. A. Yazdipour and A. Heidarzadeh, Dissimilar Butt Friction Stir Welding of Al 5083-H321 and 316L Stainless Steel Alloys, *Int. J. Adv. Manuf. Technol.*, 2016, **87**(9), p 3105–3112
14. A. Heidarzadeh, T. Saeid, and V. Klemm, Microstructure, Texture, and Mechanical Properties of Friction Stir Welded Commercial Brass Alloy, *Mater. Charact.*, 2016, **119**, p 84–91
15. A. Heidarzadeh and T. Saeid, On the Effect of β Phase on the Microstructure and Mechanical Properties of Friction Stir Welded Commercial Brass Alloys, *Data Brief*, 2015, **5**, p 1022–1025
16. M. Akbari et al. Multicriteria Optimization of Mechanical Properties of Aluminum Composites Reinforced with Different Reinforcing Particles Type, in *Proceedings of the Institution of Mechanical Engineers, Part E: Journal of Process Mechanical Engineering* (2017), p. 0954408917704994
17. P. Asadi et al. Optimization of AZ91 Friction Stir Welding Parameters Using Taguchi Method, in *Proceedings of the Institution of Mechanical Engineers, Part L: Journal of Materials Design and Applications* (2015)
18. P. Asadi, M.K.B. Givi, and M. Akbari, Simulation of Dynamic Recrystallization Process During Friction Stir Welding of AZ91 Magnesium Alloy, *Int. J. Adv. Manuf. Technol.*, 2016, **83**(1–4), p 301–311
19. R.F. Haglund et al., Nonlinear Optical Properties of Metal-Quantum-Dot Composites Synthesized by Ion Implantation, *Nucl. Instrum. Method Phys. Res. Sect. B*, 1994, **91**(1), p 493–504
20. E. Chang et al., Plasma Spraying of Zirconia-Reinforced Hydroxyapatite Composite Coatings on Titanium: Part I, Phase, Microstructure and Bonding Strength, *J. Mater. Sci. Mater. Med.*, 1997, **8**(4), p 193–200
21. X. Nie, A. Leyland, and A. Matthews, Deposition of Layered Bioceramic Hydroxyapatite/TiO2 Coatings on Titanium Alloys Using a Hybrid Technique of Micro-Arc Oxidation and Electrophoresis, *Surf. Coat. Technol.*, 2000, **125**(1–3), p 407–414
22. S. Zhou et al., Analysis of Crack Behavior for Ni-Based WC Composite Coatings by Laser Cladding and Crack-Free Realization, *Appl. Surf. Sci.*, 2008, **255**(5), p 1646–1653
23. Y. Zhao et al., Effect of Friction Stir Processing with B4C Particles on the Microstructure and Mechanical Properties of 6061 Aluminum Alloy, *Int. J. Adv. Manuf. Technol.*, 2015, **78**(9), p 1437–1443
24. P. Asadi et al., Predicting the Grain Size and Hardness of AZ91/SiC Nanocomposite by Artificial Neural Networks, *Int. J. Adv. Manuf. Technol.*, 2012, **63**(9–12), p 1095–1107
25. M.H. Shojaeefard et al. Effect of Tool Pin Profile on Distribution of Reinforcement Particles During Friction Stir Processing of B4C/Aluminum Composites, in *Proceedings of the Institution of Mechanical Engineers, Part L: Journal of Materials Design and Applications* (2016)
26. P. Asadi, M. Akbari, and H. Karimi-Nemch, 12—Simulation of Friction Stir Welding and Processing, *Advances in Friction-Stir Welding and Processing*, M.K.B. Givi and P. Asadi, Ed., Woodhead Publishing, Cambridge, 2014, p 499–542
27. J. Marzbanrad et al. Characterization of the Influence of Tool Pin Profile on Microstructural and Mechanical Properties of Friction Stir Welding, Metall. Mater. Trans. B (2014). (**In press**)
28. P. Asadi, M.B. Givi, and M. Akbari, Microstructural Simulation of Friction Stir Welding Using a Cellular Automaton Method: A Microstructure Prediction of AZ91 Magnesium Alloy, *Int. J. Mech. Mater. Eng.*, 2015, **10**(1), p 1–14
29. M.H. Shojaeefard et al., Modelling and Pareto Optimization of Mechanical Properties of Friction Stir Welded AA7075/AA5083 Butt Joints Using Neural Network and Particle Swarm Algorithm, *Mater. Des.*, 2013, **44**, p 190–198
30. M.H. Shojaeefard et al., Optimization of Microstructural and Mechanical Properties of Friction Stir Welding Using the Cellular Automaton and Taguchi Method, *Mater. Des.*, 2014, **64**, p 660–666
31. M. Shojaeefard, M. Akbari, and P. Asadi, Multi Objective Optimization of Friction Stir Welding Parameters Using FEM and Neural Network, *Int. J. Precis. Eng. Manuf.*, 2014, **15**(11), p 2351–2356
32. M.H. Shojaeefard, M. Akbari, P. Asadi, and A. Khalkhali, The Effect of Reinforcement Type on The Microstructure, Mechanical Properties, and Wear Resistance of A356 Matrix Composites Produced by FSP, *Int. J. Adv. Manuf. Technol.*, 2017, **91**(1–4), p 1391–1407
33. A.K. Kuruvilla et al., Effect of Different Reinforcements on Composite-Strengthening in Aluminium, *Bull. Mater. Sci.*, 1989, **12**(5), p 495–505
34. M. Akbari et al. The Effect of In-Process Cooling Conditions on Temperature, Force, Wear Resistance, Microstructural, and Mechanical Properties of Friction Stir Processed A356, in *Proceedings of the*

Institution of Mechanical Engineers, Part L: Journal of Materials Design and Applications (2016)

35. P. Asadi, R.A. Mahdavinejad, and S. Tutunchilar, Simulation and Experimental Investigation of FSP of AZ91 Magnesium Alloy, *Mater. Sci. Eng. A*, 2011, **528**(21), p 6469–6477

36. M. Assidi et al., Friction Model for Friction Stir Welding Process Simulation: Calibrations from Welding Experiments, *Int. J. Mach. Tools Manuf.*, 2010, **50**(2), p 143–155

37. M.H. Shojaeefard et al. Investigation of Friction Stir Welding Tool Parameters Using FEM and Neural Network, in *Proceedings of the Institution of Mechanical Engineers, Part L: Journal of Materials Design and Applications* (2013)

38. P. Asadi, M.K.B. Givi, and M. Akbari, Microstructural Simulation of Friction Stir Welding Using a Cellular Automaton Method: A Microstructure Prediction of AZ91 Magnesium Alloy, *Int. J. Mech. Mater. Eng.*, 2015, **10**(1), p 20

39. A. Mazahery and M.O. Shabani, Mechanical Properties of Squeeze-Cast A356 Composites Reinforced with B4C Particulates, *J. Mater. Eng. Perform.*, 2012, **21**(2), p 247–252

40. S.A. Sajjadi, H.R. Ezatpour, and M.T. Parizi, Comparison of Microstructure and Mechanical Properties of A356 Aluminum Alloy/Al2O3 Composites Fabricated by Stir and Compo-Casting Processes, *Mater. Des.*, 2012, **34**, p 106–111

41. O. Carvalho et al., Evaluation of CNT Dispersion Methodology Effect on Mechanical Properties of an AlSi Composite, *J. Mater. Eng. Perform.*, 2015, **24**(6), p 2535–2545

42. H. Izadi et al., Friction Stir Processing of Al/SiC Composites Fabricated by Powder Metallurgy, *J. Mater. Process. Technol.*, 2013, **213**(11), p 1900–1907

43. A. Mostafa et al., A Cellular Automaton Model for Microstructural Simulation of Friction Stir Welded AZ91 Magnesium Alloy, *Modell. Simul. Mater. Sci. Eng.*, 2016, **24**(3), p 035012

44. S. Sahraeinejad et al., Fabrication of Metal Matrix Composites by Friction Stir Processing with Different Particles and Processing Parameters, *Mater. Sci. Eng. A*, 2015, **626**, p 505–513

45. A. Mazahery, M. Alizadeh, and M.O. Shabani, Study of Tribological and Mechanical Properties of A356—Nano SiC Composites, *Trans. Indian Inst. Met.*, 2012, **65**(4), p 393–398

46. A. Mazahery and M.O. Shabani, Microstructural and Abrasive Wear Properties of SiC Reinforced Aluminum-Based Composite Produced by Compocasting, *Trans. Nonferr. Met. Soc. China*, 2013, **23**(7), p 1905–1914

47. T.S. Mahmoud, Surface Modification of A390 Hypereutectic Al-Si Cast Alloys Using Friction Stir Processing, *Surf. Coat. Technol.*, 2013, **228**, p 209–220

48. M.O. Shabani and A. Mazahery, Application of GA to Optimize the Process Conditions of Al Matrix Nano-Composites, *Compos. B Eng.*, 2013, **45**(1), p 185–191

49. A.T. Alpas and J. Zhang, Effect of SiC Particulate Reinforcement on the Dry Sliding Wear of Aluminium-Silicon Alloys (A356), *Wear*, 1992, **155**(1), p 83–104

50. M. Uthayakumar, S. Aravindan, and K. Rajkumar, Wear Performance of Al-SiC-B4C Hybrid Composites Under Dry Sliding Conditions, *Mater. Des.*, 2013, **47**, p 456–464

51. N. Natarajan, S. Vijayarangan, and I. Rajendran, Wear Behaviour of A356/25SiCp Aluminium Matrix Composites Sliding Against Automobile Friction Material, *Wear*, 2006, **261**(7–8), p 812–822